J. Fluid Mech. (1994), *vol.* 272, *pp.* 45–65

The solidification of buoyancy-driven flow in a flexible-walled channel. Part 2. Continual release

By JOHN R. LISTER

Institute of Theoretical Geophysics, Department of Applied Mathematics and Theoretical Physics, University of Cambridge, Silver Street, Cambridge CB3 9EW, UK

(Received 9 March 1993 and in revised form 24 January 1994)

The model developed in Part 1 (Lister 1994) for the solidification of hot fluid flowing in a thin buoyancy-driven layer between cold solid but freely deformable boundaries is extended to study the case of continual release of fluid. In this model lubrication theory was applied to reduce the equations of mass and heat conservation to a kinematic-wave equation and an advection–diffusion equation, which were coupled by the rate of solidification. The equations allow the source flux to be specified, and the cases of constant input and of flux proportional to a power of time are considered here. The structure of the flow differs significantly from the case of constant-volume release considered in Part 1. The advective resupply of heat prevents the flow from solidifying completely at the source and, if the initial fluid temperature is greater than the melting temperature of the solid, will in fact lead to rapid melting near the source. A perturbation expansion is used to describe the development of thermal boundary layers at the flow margins and the initial self-similar extension of the zone of melting. As the flow propagates beyond its thermal entry length, the fluid temperature falls to the liquidus value and melting gives way to solidification. At large times nearly all of the fluid supplied solidifies against the margins of the flow but, provided the source flux decreases less rapidly than $t^{-1/2}$, sufficient reaches the nose of the flow that the flow continues to increase in length indefinitely. Analytic solutions are given for this long-time regime showing, for example, that the length increases asymptotically like $t^{1/2}$ for constant-flux input. The theoretical solutions, which are calculated by a combination of analytic and numerical methods, may be used to describe the propagation of a dyke fed by a large body of magma through the Earth's lithosphere or the flow of lava down the flanks of a volcano during an extensive period of eruption.

1. Introduction

In Part 1 (Lister 1994) we posed the general question: how far can a hot fluid flow into cold surroundings before it solidifies and flow ceases? The question is highly pertinent to the transport of hot magma through fissures, or dykes, in the Earth's cold lithosphere and to the flow of lavas on the Earth's surface. Previous dynamical analyses (Spence & Turcotte 1990; Lister 1990*a*, *b*) show that the flow of magma in dykes can be described as buoyancy-driven flow between freely deformable boundaries and in Part 1 the equations governing the thermal evolution and solidification of two-dimensional flow in a flexible-walled channel were derived. The equations were solved for the case of an instantaneous line release of constant volume and it was shown that such a flow will come to rest and solidify completely in a finite distance, which was evaluated. In this paper we derive solutions for the case of continual input and show that propagation of the flow can continue indefinitely, though at a rate which is much

reduced from the rate without solidification. Though the equations differ only in the source-flux boundary condition, the structure of the solutions for continual input is found to be quite different from that for instantaneous release and consequently requires new analysis.

Many early studies of the solidification of dykes (see the review by Delaney 1987) have been based on solutions for unsteady heat conduction from a stationary body of magma brought instantaneously into contact with cooler host rock. For example, in order to obtain a rough estimate of the distance propagated before solidification, the unidirectional solidification time for a stationary constant-thickness slab of fluid was multiplied by the mean velocity of flow corresponding to the original width. The dynamic coupling between the effects of solidification on the flow and of advection of heat by the flow on the solidification was first estimated by Delaney & Pollard (1982). They approximated flow in a rigid-walled conduit by Poiseuille flow with a spatially constant pressure gradient (which violates mass conservation if the channel width varies) and neglected the effects of latent heat. The thermal evolution and migration of the solidification isotherm was then calculated using a truncated series expansion of the thermal boundary-layer equations (Leveque 1928; Newmann 1969). Bruce & Huppert (1989, 1990) derived a more sophisticated approximation for flow in a finite-length rigid-walled channel by assuming that the flow rate is governed only by the time-dependent width at the top of the channel. The thermal calculation, which included the effects of latent heat, was based on a quasi-steady analysis of slowly varying linear shear in the thermal boundary layers on the walls. Both these analyses of flows in a rigid-walled channel concluded that flow would eventually cease if the conduit exceeded a critical length. By contrast, we show below that flow in a flexible-walled channel can continue indefinitely unless the source flux abates.

A model of flow in a flexible-walled channel was developed in Part 1 and the reader is referred there for details of the derivation and the conditions under which the underlying assumptions are valid. Nevertheless, it is hoped that the present paper can be read independently and accordingly the dimensionless form of the governing equations is summarized below for reference in the subsequent analysis.

The velocity $\boldsymbol{u}$ is given by Poiseuille flow coupled to the lateral displacement of the channel walls by conservation of mass. Hence

$$\boldsymbol{u} = (-ww_z x, \tfrac{1}{2}(w^2 - x^2)) \quad (0 \leqslant x \leqslant w), \tag{1.1a}$$

$$\boldsymbol{u} = (-w^2 w_z, 0) \qquad (w \leqslant x), \tag{1.1b}$$

$$w_t + w^2 w_z + c_t = 0 \tag{1.2}$$

(together with symmetry in $x = 0$), where the fluid region occupies $|x| \leqslant w(z, t)$ for $0 \leqslant z \leqslant z_N(t)$; x is the cross-stream coordinate, z the vertical coordinate, $z = 0$ the level of release, $z = z_N(t)$ the nose of the flow and $c_t(z, t)$ the local rate of solidification. The high-Péclet-number thermal transport is governed by advection and cross-stream diffusion subject to Stefan boundary conditions at the walls and to far-field boundary conditions. Thus

$$\theta_t + \boldsymbol{u} \cdot \nabla\theta = \theta_{xx}, \tag{1.3}$$

$$Sc_t + [\theta_x(w, z, t)]^+_- = 0, \tag{1.4}$$

$$\theta(w, z, t) = \Theta, \tag{1.5}$$

$$\theta(x, z, t) \to 0 \quad (x \to \infty), \tag{1.6}$$

where the parameters

$$S = \frac{L}{C_p(T_0 - T_\infty)} \tag{1.7a}$$

$$\Theta = \frac{T_L - T_\infty}{T_0 - T_\infty}, \tag{1.7b}$$

are the Stefan number and dimensionless solidification temperature, T_0 and T_∞ are the (dimensional) initial temperatures of fluid and solid, T_L is the liquidus temperature, L is the latent heat and C_p the specific heat capacity. Heat and mass conservation at the nose of the flow show that

$$\mathrm{d}z_N/\mathrm{d}t = \tfrac{1}{3}w_N^2, \tag{1.8}$$

$$c(z_N, t) = 0, \tag{1.9}$$

$$\theta(x, z_N, t) = \theta(\tilde{x}(x), z_N, t) \quad (w_N/\sqrt{3} < x < w_N), \tag{1.10a}$$

$$\theta(x, z_N, t) = 0, \qquad (w_N < x), \tag{1.10b}$$

where $\tilde{x}(x)$ is the positive root of

$$\tilde{x}^2 + x\tilde{x} + x^2 = w_N^2. \tag{1.11}$$

The initial and source conditions, which differ from Part 1, are prescribed by

$$z_N(0) = 0, \tag{1.12}$$

$$\theta(x, 0, t) = 1 \quad (x < w(0, t)), \tag{1.13}$$

$$w(0, t) = t^\alpha, \tag{1.14}$$

where $\alpha = 0$ corresponds to the important case of constant-flux release. The non-dimensionalization is defined by equations (2.14) and (2.15) of Part 1, where the reference width h_0 is chosen to produce (1.14). The z-scale is the thermal entry length $Pe\,h_0$, where the Péclet number satisfies $Pe \gg 1$.

In §2 we solve (1.1)–(1.14) for the simplest case of constant-flux input at the liquidus temperature ($\alpha = 0$, $\Theta = 1$). It is shown that at short times $z_N \propto t$ and at long times $z_N \propto t^{1/2}$. Analytic solutions are found in each regime and the full evolution of the flow is calculated by a method of characteristics. Unlike the cases of constant-volume release and of continual release above the liquidus temperature, no special treatment is needed to obtain the solution near the origin of the flow. In §3 we extend our analysis to constant-flux input above the liquidus temperature ($\Theta < 1$). We find that a zone of melting extends from the source and grows like $t^{3/2}$ until it reaches the thermal entry length. Beyond this distance the fluid has lost its superheat and the flow is given by a rescaling of the $\Theta = 1$ solution. The case of non-constant input is considered in §4 and a condition for indefinite propagation derived. The results are discussed in §5.

2. Constant-flux input at the liquidus temperature

We consider the solution of (1.1)–(1.14) for $\alpha = 0$ and $\Theta = 1$. Since the fluid source temperature at $z = 0$ is equal in this case to the temperature at the boundaries $x = \pm w$, the temperature of the fluid region remains uniform and equal to the liquidus value $\theta = 1$. The temperature of the solid at a given height is zero until the nose of the flow reaches that height at time $t_N(z)$. From then on, as shown in Part 1, the temperature in the solid is given by the usual error-function solution for one-dimensional solidification of a liquid placed in contact with a semi-infinite cold solid (Carslaw & Jaeger 1959), but with a lateral displacement given by (1.1*b*). Thus

$$c_t = \lambda(S)/(t - t_N)^{1/2} \tag{2.1}$$

for $t > t_N$, where

$$S\pi^{1/2}\lambda\, e^{\lambda^2}\operatorname{erfc}(-\lambda) = 1. \tag{2.2}$$

The mass transport of the flow is then given by substitution of (2.1) into (1.2). In order to include the possibility of turbulent flow, for which the mass flux is proportional to w^{n+1} with $n < 2$ (Hirs 1974), we generalize (1.2) and (1.8) to

$$w_t + w^n w_z = -\lambda/[t - t_N(z)]^{1/2}, \tag{2.3}$$

$$dz_N/dt = w_N^n/(n+1) \tag{2.4}$$

(Lister 1994). The departure of a turbulent velocity profile from (1.1*a*) is immaterial to the thermal solution because the fluid temperature is constant if $\Theta = 1$.

The remaining parameter λ is scaled out of the problem by defining

$$Z = z\lambda^2, \quad W = w, \quad T = t\lambda^2. \tag{2.5}$$

Equation (2.3) is most easily solved by the method of characteristics, which we label by the variable ϕ. Hence

$$\left(\frac{\partial Z}{\partial T}\right)_\phi = W^n, \quad \left(\frac{\partial W}{\partial T}\right)_\phi = -\frac{1}{[T - T_N(Z)]^{1/2}}, \tag{2.6a, b}$$

$$Z(T_S;\phi) = 0, \quad W(T_S;\phi) = 1, \tag{2.6c, d}$$

where T_S is the time at which the characteristic $Z(T;\phi)$ crosses $Z = 0$. Clearly,

$$W(T;\phi) = 1 - \int_{T_S}^{T} \frac{dv}{(v - T_N[Z(v;\phi)])^{1/2}}. \tag{2.7}$$

2.1. *Short-time expansion*

We seek a series solution of (2.6) at short times. It is convenient to define the label of the characteristics by $\phi^2 = T_N - T_S$, where $T_N(\phi)$ is the time at which the characteristic ϕ reaches the nose of the flow. A stretched time variable is defined by $\tau(\phi) = (T - T_S)/\phi^2$ in order to fix the source of the flow at $\tau = 0$ and the nose at $\tau = 1$. Hence, we write

$$T - T_N(Z) = \phi^2(\tau - 1) + T_N(\phi) - T_N(Z) \tag{2.8}$$

in the integrand of (2.7).

We pose expansions

$$\phi^{-2}Z(\tau;\phi) = Z^*(\tau;\phi) = Z_0(\tau) + \phi Z_1(\tau) + \ldots, \tag{2.9a}$$

$$\phi^{-2}T_N(\phi) = T_N^* = (n+1)(T_0 + \phi T_1 + \ldots), \tag{2.9b}$$

$$\phi_N(Z) = Z^{1/2}(\phi_0 + \phi_1 Z^{1/2} + \phi_2 Z + \ldots) = \phi Z^{*1/2}(\phi_0 + \phi_1 \phi Z^{*1/2} + \phi_2 \phi^2 Z^* + \ldots) \tag{2.9c}$$

for the unknowns $Z(\tau;\phi)$, $T_N(\phi)$ and the inverse $\phi_N(Z)$ of $Z_N(\phi)$. On substitution of the starred variables into (2.4), (2.6*a*) and (2.7), we obtain

$$\frac{\partial Z^*}{\partial \tau} = \left(1 - \phi \int_0^\tau \frac{dv}{[v - 1 + T_N^*(\phi) - T_N(\phi_N[Z])/\phi^2]^{1/2}}\right)^n, \tag{2.10a}$$

$$(n+1)\frac{dZ(1;\phi)}{d\phi} = \frac{dT_N}{d\phi}\left(1 - \phi \int_0^1 \frac{dv}{[v - 1 + T_N^*(\phi) - T_N(\phi_N[Z])/\phi^2]^{1/2}}\right)^n, \tag{2.10b}$$

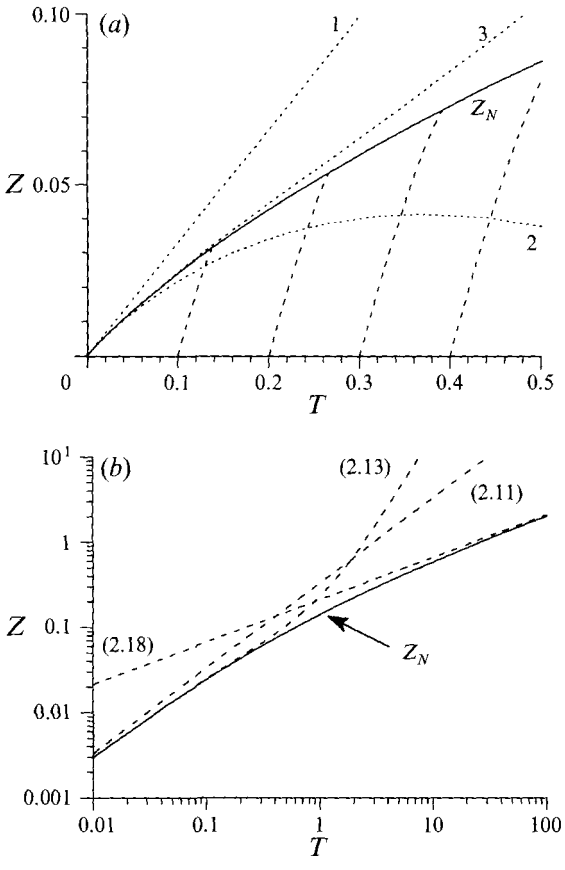

FIGURE 1. (*a*) The propagation of the nose of a constant-input laminar flow at the liquidus temperature ($\alpha = 0$, $n = 2$ and $\Theta = 1$, solid curve) together with the first three short-time asymptotic approximations (2.11)–(2.13) (dotted). The solution was determined by a modified method of characteristics some of which are shown dashed. (*b*) The rate of propagation decreases steadily so that initial advance with $Z_N \propto T$ (2.11) gives way to a long-time advance with $Z_N \propto T^{1/2}$. There is good agreement with the asymptotic solutions (2.13) and (2.18).

and we also have the identity

$$\phi_N(Z(1;\phi)) \equiv \phi. \tag{2.10c}$$

The form of (2.10) shows that the scaling of the series expansions (2.9) in powers of ϕ is correct. The coefficients $Z_i(\tau)$, T_i and ϕ_i are determined by solution at successive order.

At leading order we obtain

$$Z_0(\tau) = \tau, \quad T_0 = 1, \quad \phi_0 = 1, \tag{2.11}$$

which corresponds to the simple loss-less kinematic shock wave $W = 1$ in $0 < Z < Z_N = T/(n+1)$. The first effects of solidification occur at $O(\phi)$. We find from (2.11*a*) that

$$v - 1 + T_N^*(\phi) - T_N(\phi_N[Z])/\phi^2 = n(1-T) + O(\phi),$$

allowing the integrals in (2.10) to be easily evaluated. The $O(\phi)$ solutions are

$$Z_1(\tau) = \tfrac{2}{3}n^{1/2}(2 - 3\tau - 2(1-\tau)^{3/2}), \quad T_1 = \tfrac{2}{3}n^{1/2}, \quad \phi_1 = \tfrac{1}{3}n^{1/2}. \tag{2.12}$$

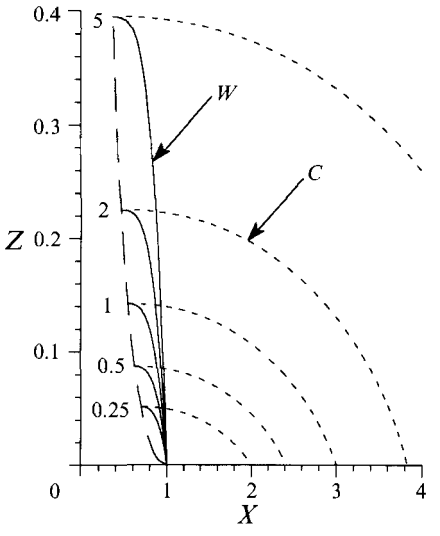

FIGURE 2. The scaled width W (solid curves), the accumulated chill thickness C (dashed) and the width at the nose W_N (long dashed) obtained from (2.4) and (2.6) as a function of vertical distance Z at times $T = 0.25$, 0.5, 1, 2 and 5. The effects of solidification are strongest near the nose where the temperature gradients are steep.

Higher-order solutions are similarly easily calculated, though the algebra becomes rather tedious. The location of the nose can be found by reversion of the series $T = T_N(\phi_N[Z])$ to be

$$Z_N = \frac{T}{n+1} - \frac{4n^{1/2}}{3}\left(\frac{T}{n+1}\right)^{3/2} + \frac{3\pi(n+1)-14}{6}\left(\frac{T}{n+1}\right)^2 + O(T^{5/2}). \tag{2.13}$$

2.2. *Numerical solution*

As might be expected, the short-time analysis shows that the solidification causes the propagation velocity to decrease with time, and the initial decrease has been evaluated above. The behaviour at moderate to long times is not obvious *a priori*. Naive guesses that the flow will propagate a finite distance before the nose solidifies completely or that some sort of steady state is established with propagation at a reduced but constant velocity are found to be incorrect.

The general solution of (2.3) and (2.4) was determined by a fourth-order Runge–Kutta integration of (2.6) using for the discretization of $T_N(Z)$ a sequence of quadratic segments each of which was constrained to satisfy (2.4) at its endpoints. Further details of the numerical scheme are given in Part 1. The propagation of the nose of the flow together with some of the characteristics at early times is shown in figure 1 (*a*) for $n = 2$. The slope of the characteristics is 1 at $Z = 0$ and three times that of the frontal trajectory at their intersection. Continued integration shows that the length of the flow at large times is proportional to $T^{1/2}$ (figure 1 *b*). Thus $W(Z_N)$ and the rate of propagation are monotonically decreasing like $T^{-1/2}$ and never reach zero. The explanation of this result is deferred to the following section after derivation of the asymptotic solution for the long-time regime. In figure 2 we show the widths of the flow W and of the accumulated chill C at a succession of times. Though the width at the nose of the flow is monotonically decreasing, the width at any given location is monotonically increasing.

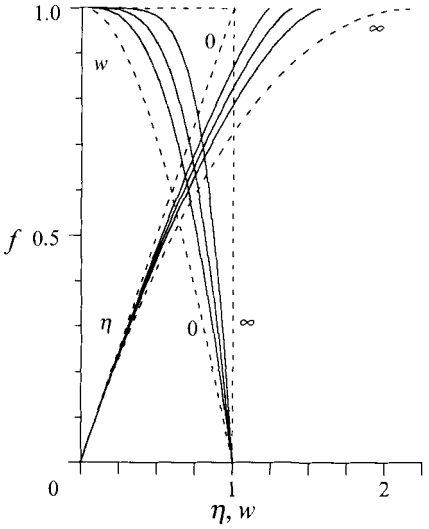

FIGURE 3. The asymptotic similarity solution (2.14) for the characteristic trajectory and width w at long times, where f is the scaled vertical coordinate and η is the scaled time variable along a characteristic. The solid curves correspond to the solutions for $n = \frac{1}{2}$, 1 and 2 and the dashed curves to the limiting solutions for $n = 0$ and $n = \infty$.

2.3. *The long-time solution*

The numerical solution shows that

$$T_N \sim k^2 Z^2 \tag{2.14a}$$

as $Z \to \infty$, where k is a constant. From figure 2 we see that $W = O(1)$ except very close to the nose of the flow. Hence, if $Z_N \sim T^{1/2}/k$ then $T_N - T_S = O(T^{1/2}/k) \ll T$. This suggests that we seek a solution to (2.4) and (2.6) of the form

$$Z(T; T_S) = T_S^{1/2} f(\eta)/k, \tag{2.14b}$$

where

$$\eta = k(T - T_S)/T_S^{1/2}. \tag{2.14c}$$

We write $T = T_S + O(T_S^{1/2})$ in (2.6b), note that $f' = (n+1)\,\mathrm{d}Z_N/\mathrm{d}T = O(T_S^{-1/2})$ at the nose and substitute (2.14) into (2.6) to obtain

$$\frac{kf''}{n(f')^{1-1/n}} = -\frac{1}{(1-f^2)^{1/2}} + O(T_S^{-1/2}) \tag{2.15}$$

subject to the boundary conditions

$$f(0) = 0, \quad f'(0) = 1, \quad f(\eta_N) = 1, \quad f'(\eta_N) = 0, \tag{2.16a–d}$$

where primes denote derivatives with respect to η. Equation (2.15) has the first integral

$$\left[\frac{k(f')^{(1/n)+1}}{n+1}\right] = [\cos^{-1} f] \tag{2.17}$$

from which we can use (2.16) to obtain $k = \frac{1}{2}\pi(n+1)$. Thus

$$Z_N \sim \frac{2T^{1/2}}{\pi(n+1)}, \tag{2.18}$$

in agreement with the numerical results of figure 1(b). The characteristic equation

$$f' = \{2\cos^{-1}(f)/\pi\}^{n/(n+1)}$$

can be integrated analytically by the substitution $v = 2\cos^{-1}(f)/\pi$ (Gradshteyn & Ryzhik 1980, equation 2.632.2) and the solution and the asymptotic form of W are shown in figure 3 for a number of values of n. As n increases the dependence of $\mathrm{d}Z/\mathrm{d}T$ on W becomes stronger and the effects of solidification are increasingly confined to the nose. Hence the decrease in W at the nose of the flow is sharper for laminar flows ($n = 2$) than for turbulent flows ($n < 2$).

The dominant balance which gives rise to the long-term asymptotic behaviour is now clear. Nearly all of the input flux, which is constant, solidifies against the side boundaries. Since the rate of solidification decreases like $T^{-1/2}$ as the temperature gradient in the solid spreads, the length of the flow increases like $T^{1/2}$ to compensate. Just sufficient of the input flux reaches the nose of the flow to keep it open and propagating at the appropriate rate. The indefinite propagation of a constant-input flow contrasts with the finite distance of propagation of a fixed-volume release (Lister 1994) and will be discussed in §5.

3. Constant-flux input above the liquidus temperature

We have seen that if $\Theta = 1$ then solidification proceeds along the entire length of the flow and no special treatment of the near-source region is necessary. If $\Theta < 1$, however, then we would expect the continual supply of fluid at temperature 1 at $z = 0$ to lead to a region of wall melting near the source. The description of the near-source melting will be the focus of the analysis below since the far-field region of solidification is found to be similar to the liquidus solutions of the previous section.

3.1. *The solution at short times*

Shortly after the initiation of flow the temperature gradient between fluid and solid is confined to thermal boundary layers of width $\delta = O(t^{1/2})$ at the margins $x = \pm w$ of the flow. Since the centreline velocity is initially $O(1)$, the boundary layers are subject only to velocities $O(\delta)$ in the shear flow at the edge of the Poiseuille profile. Except very near the source of the flow, the along-stream scale of temperature variation is $z_N = O(t)$. Thus the ratio of advection to diffusion $u\theta_z/\theta_{xx}$ in (1.1) is $O(t^{-1/2})$. Hence, if we calculate the rate of solidification by conduction alone then the associated error is of relative size $O(t^{-1/2})$. Now when a semi-infinite body of fluid of initial temperature $\theta = 1$ is placed in contact with a semi-infinite solid of initial temperature $\theta = 0$ at $t = t_N$, the rate of solidification is given by

$$c_t = \lambda(S, \Theta)/(t - t_N)^{1/2} \tag{3.1}$$

for $t > t_N$ (Carslaw & Jaeger 1959), where $\lambda(S, \Theta)$ is the root of

$$S\pi^{1/2}\lambda\,\mathrm{e}^{\lambda^2} = \frac{\Theta}{\operatorname{erfc}(-\lambda)} - \frac{(1-\Theta)}{\operatorname{erfc}\lambda}. \tag{3.2}$$

Since $\delta \ll w$, the correction due to the finite width of the flow is negligible. Thus the perturbation analysis of §2.1 restricted to laminar flow ($n = 2$) is applicable to second order, and we again obtain (2.11) and (2.12). The location of the nose is given by

$$z_N = \tfrac{1}{3}t - \tfrac{2}{3}\lambda(\tfrac{2}{3}t)^{3/2} + O(t^2), \tag{3.3}$$

where it is necessary to include the effects of advection on the thermal boundary layers to calculate the higher-order terms.

Advection must also be included near the origin of the flow. For $z \ll z_N$ the

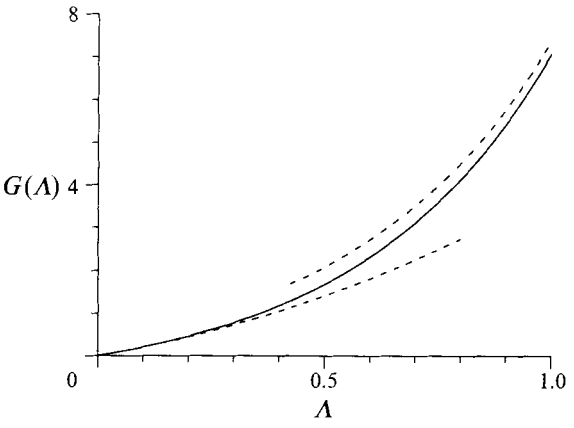

FIGURE 4. The function $G(\Lambda) = \Lambda \int_0^\infty \exp(\Lambda\eta - \frac{1}{9}\eta^3)\,\mathrm{d}\eta$ which determines Λ in the steady near-source similarity solution (3.10) at short times from the condition $G(\Lambda) = (1-\Theta)/(S+\Theta)$. The asymptotic approximations $G \sim 3^{-1/3}\Gamma(\frac{1}{3})\Lambda + 3^{1/3}\Gamma(\frac{2}{3})\Lambda^2$ as $\Lambda \to 0$ and $G \sim (3\pi^2\Lambda^3)^{1/4}\exp[(\frac{4}{3}\Lambda^3)^{1/2}]$ as $\Lambda \to \infty$ are shown dashed.

temperature profiles corresponding to the purely conductive approximation used above are given by

$$\theta \sim \frac{\Theta\,\mathrm{erfc}\{-(\frac{1}{2}\xi+\lambda)\}}{\mathrm{erfc}(-\lambda)} \qquad (\xi \leqslant 0), \tag{3.4a}$$

$$\theta \sim 1 - \frac{(1-\Theta)\,\mathrm{erfc}\{\frac{1}{2}\xi+\lambda\}}{\mathrm{erfc}\,\lambda}, \quad (\xi \geqslant 0), \tag{3.4b}$$

where $\xi = (w-x)/t^{1/2}$ (see equation (4.3) of Part 1). At $z = 0$, however, we must apply the boundary condition $\theta = 1$ in $\xi > 0$ from (1.13). It follows that there is a small region near the source in which the along-stream scale of temperature variation is much less than z_N, θ_z cannot be neglected and the temperature is matched from (1.13) to (3.4). Within this small region the curvature of the Poiseuille profile can be neglected and (1.3) written

$$\theta_t - c_t\theta_{x'} + x'\theta_z = \theta_{x'x'} \quad (x' > 0), \tag{3.5}$$

where $x' = w-x$.

The lack of a lengthscale in (3.5) suggests that we seek a similarity solution of the form

$$\theta(x,z,t) = \vartheta(\xi,\zeta), \quad c_t = t^{-1/2}v(\zeta), \tag{3.6}$$

where

$$\xi = x'/t^{1/2}, \quad \zeta = z/t^{3/2}. \tag{3.7}$$

After making these substitutions, we need to solve

$$(\xi - \tfrac{3}{2}\zeta)\vartheta_\zeta = (v+\tfrac{1}{2}\xi)\vartheta_\xi + \vartheta_{\xi\xi} \quad (\xi > 0), \tag{3.8a}$$

$$-\tfrac{3}{2}\zeta\vartheta_\zeta = (v+\tfrac{1}{2}\xi)\vartheta_\xi + \vartheta_{\xi\xi} \quad (\xi < 0), \tag{3.8b}$$

$$Sv + [\vartheta_\xi]_-^+ = 0, \tag{3.8c}$$

$$\vartheta(0,\zeta) = \Theta, \quad \vartheta(\infty,\zeta) = 1, \quad \vartheta(-\infty,\zeta) = 0, \tag{3.8d–f}$$

$$\vartheta(\xi,0) = 1 \qquad (\xi > 0) \tag{3.8g}$$

subject to the far-field condition that $v \to \lambda$ and ϑ asymptotes to (3.4) as $\zeta \to \infty$. Bruce (1989) derived similar equations for flow past a rigid wall, but neglected v in the equations corresponding to (3.8*a*, *b*) in order to obtain approximate analytic solutions.

The far-field boundary condition (3.4) is determined by a balance between cross-stream diffusion and time dependence. As $\zeta \to 0$, however, the flow must approach a steady state in which there is a balance between advection and diffusion. We see from

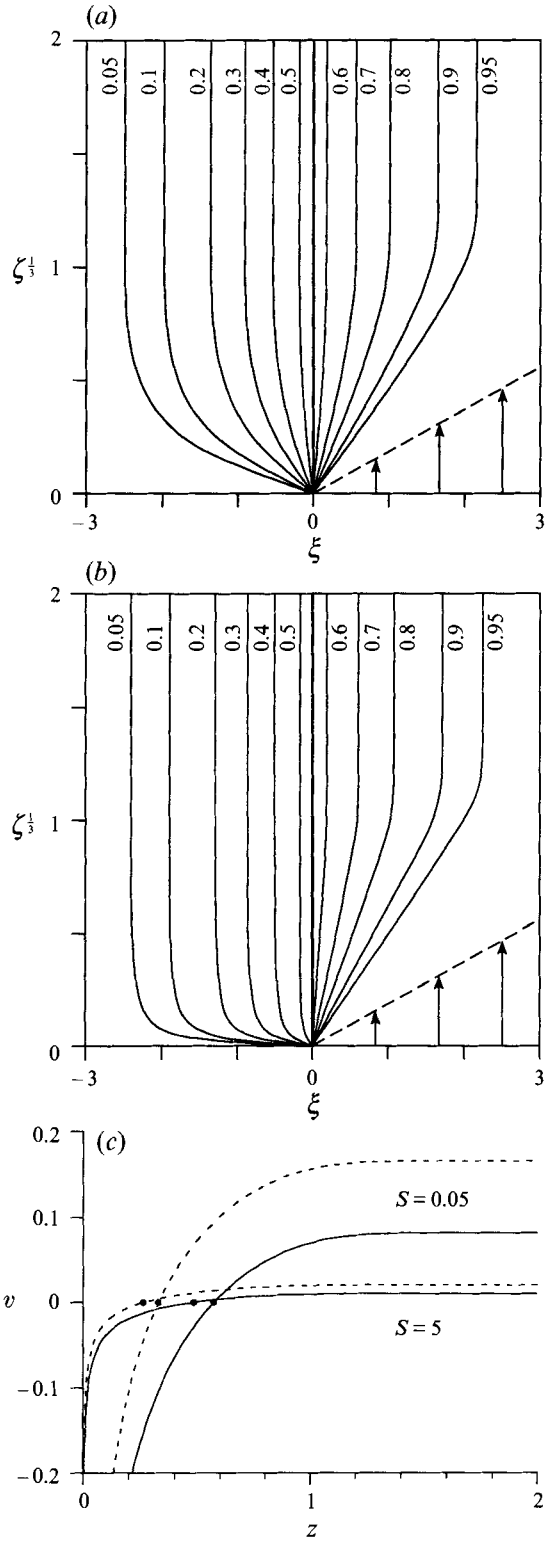

FIGURE 5 (*a–c*). For caption see facing page.

(3.7) that in a steady state ϑ is a function of $\eta = x'/z^{1/3} = \xi/\zeta^{1/3}$. Thus we substitute $\vartheta = \vartheta(\eta)$ into (3.8) and let $\zeta \to 0$ to obtain

$$(v\zeta^{1/3})\,\vartheta_\eta + \vartheta_{\eta\eta} = -\tfrac{1}{3}\eta^2\vartheta_\eta \quad (\eta > 0), \tag{3.9a}$$

$$(v\zeta^{1/3})\,\vartheta_\eta + \vartheta_{\eta\eta} = 0 \quad (\eta < 0), \tag{3.9b}$$

$$S(v\zeta^{1/3}) + [\vartheta_\eta]^+_- = 0. \tag{3.9c}$$

The solution of (3.9) subject to (3.8*d–g*) is given by

$$\vartheta(\eta) = 1 - \frac{(1-\Theta)\displaystyle\int_\eta^\infty \exp(\Lambda\eta - \tfrac{1}{9}\eta^3)\,\mathrm{d}\eta}{\displaystyle\int_0^\infty \exp(\Lambda\eta - \tfrac{1}{9}\eta^3)\,\mathrm{d}\eta} \quad (\eta \geqslant 0), \tag{3.10a}$$

$$\vartheta(\eta) = \Theta\,\mathrm{e}^{\Lambda\eta} \quad (\eta \leqslant 0), \tag{3.10b}$$

$$v = -\Lambda/\zeta^{1/3}, \tag{3.10c}$$

where Λ is given by

$$\Lambda \int_0^\infty \exp(\Lambda\eta - \tfrac{1}{9}\eta^3)\,\mathrm{d}\eta = \frac{1-\Theta}{S+\Theta}. \tag{3.10d}$$

The left-hand side of (3.10*d*) is shown in figure 4.

Thus (3.10) and (3.4) are the near-source ($\zeta \ll 1$) and far-field ($\zeta \gg 1$) solutions of (3.5). The near-source solution satisfies (3.8*a–g*) but not the far-field boundary condition (3.4). Conversely, (3.4) satisfies (3.8*a–f*) but not the source boundary condition (3.8*g*). That the full solution must satisfy both upstream and downstream boundary conditions is due to the variation in sign of the coefficient of ϑ_ζ in (3.8*a*): though the equation is parabolic, the time-like direction is $+\zeta$ in $\xi > \frac{3}{2}\zeta$ and $-\zeta$ in $\xi < \frac{3}{2}\zeta$. Such bidirectional information transport in the heat equation is characteristic of flows propagating away from a source.

The full solution of (3.8) subject to (3.4) was determined numerically using an adaptation of the scheme described in §4.3 of Part 1: a time-like derivative ϑ_τ was introduced in (3.8*a*, *b*), ξ-derivatives were represented by Crank–Nicholson discretization and ζ-derivatives by Lax–Wendroff discretization. The equations were then integrated with respect to τ to a τ-independent state, which solves the original problem. The solutions for $S = 0.05$ and $S = 5$ with $\Theta = 0.55$ are shown in figure 5(*a*, *b*). The temperature in the fluid region makes a fairly sharp transition from the near-source asymptotic (3.10) to the far-field boundary condition (3.4) near $\zeta = 1$ and depends only weakly on the Stefan number. As $S \to \infty$ the temperature in the solid region tends to the far-field error-function profile except within a small region of size $O(S^{-3})$ near the source. In the limit $S = \infty$ the solidification rate is zero, and hence the equations in the fluid and solid regions are decoupled and linear and can be solved by Laplace transforms (Appendix).

Near the origin the flow is steady and the boundary-layer thickness increases downstream; far from the origin the boundary-layer thickness is independent of downstream distance, but is thickening like $t^{1/2}$. Since $\Lambda > 0$ if $\Theta < 1$ and $\lambda > 0$ if $\Theta > \frac{1}{2}$, it follows that if $\frac{1}{2} < \Theta < 1$ then there is a transition point ζ_T between melting

FIGURE 5. Contours of temperature ϑ in the transient similarity solution (3.8) for the near-source short-time flow. The solution depends only on ξ as $\zeta \to \infty$ and on $\eta = \xi/\zeta^{1/3}$ as $\zeta \to 0$. (*a*) $S = 0.05$ and $\Theta = 0.55$; (*b*) $S = 5$ and $\Theta = 0.55$. (*c*) The solidification rate v shows a transition between near-source melting and far-field solidification if $\Theta > \frac{1}{2}$. The transition points (●) are shown for $\Theta = 0.55$ (solid curves) and $\Theta = 0.6$ (dashed curves) and for $S = 0.05$ and $S = 5$.

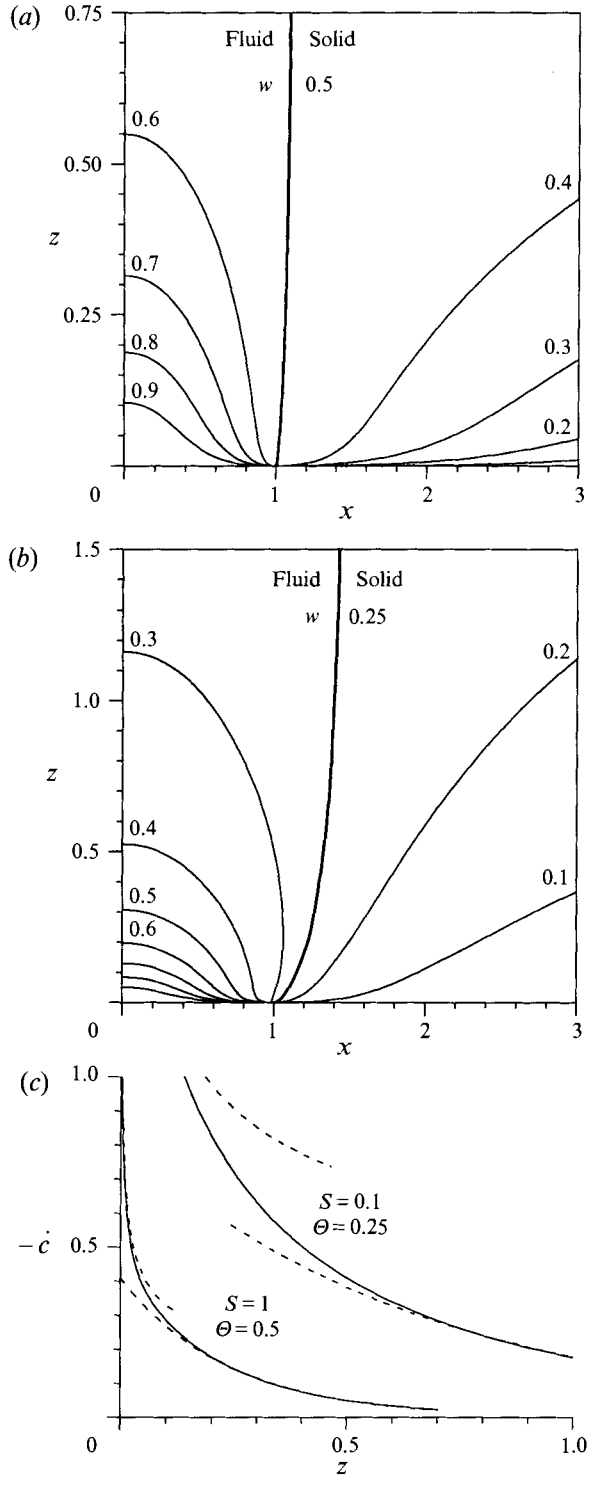

FIGURE 6. Contours of temperature θ in the steady near-source long-time solution (3.13). The temperature of both the fluid and the solid tends to Θ as $z \to \infty$ and $w \to [(S+1)/(S+\Theta)]^{1/3}$. (*a*) $S = 1$ and $\Theta = 0.5$; (*b*) $S = 0.1$ and $\Theta = 0.25$. Note the different vertical scale. (*c*) The melting rate $-\dot{c}$ (solid curves) together with the near-source and far-field asymptotic solutions $-\dot{c} = A/z^{1/3}$ and $-\dot{c} \propto \exp(-pz/w_\infty^4)$ (dashed).

($v < 0$) in $\zeta < \zeta_T$ and solidification ($v > 0$) in $\zeta > \zeta_T$ (figure 5*c*). In the original variables the region of melting extends from the origin with $z_T \propto t^{3/2}$. It should be noted that this whole picture is a local solution which applies for $z \ll z_N$ and $x' \ll w$. For consistency with (3.7), we also require $t \ll 1$.

3.2. *Long-time solution*

When $t = O(1)$ we can no longer use a match of the perturbation solution (3.3) to the near-source similarity solution (3.8), and the original equations (1.1)–(1.14) must be solved numerically. At long times ($t \gg 1$), however, the problem simplifies again and we may make further progress analytically. We have shown above that the solution of (3.5) becomes steady near the source in a region that grows like $t^{3/2}$ at short times. This suggests that we seek a steady near-source solution to (1.1)–(1.14) that is valid for $t \gg 1$.

Accordingly, we write the solidification rate c_t (which is negative) as $\dot{c}(z)$ and set $\theta_t = 0$ and $w_t = 0$. From (1.1*b*), (1.2) and (1.3) we obtain

$$\dot{c}\theta_x = \theta_{xx} \quad (x > w) \tag{3.11}$$

which has solution

$$\theta = \Theta \, \mathrm{e}^{\dot{c}(x-w)} \quad (x \geqslant w) \tag{3.12}$$

subject to the boundary conditions $\theta = \Theta$ at $x = w$ and $\theta \to 0$ as $x \to \infty$. Substitution into the remaining equations yields the system

$$\tfrac{1}{2}(w^2 - x^2)\theta_z = \theta_{xx} - (\dot{c}x/w)\theta_x, \quad (x < w), \tag{3.13a}$$

$$w_z = -\dot{c}/w^2, \tag{3.13b}$$

$$\dot{c} = \theta_{x-}/(S + \Theta), \tag{3.13c}$$

which is to be solved subject to the boundary conditions $w = 1$ and $\theta = 1$ at $z = 0$ and $\theta = \Theta$ at $x = w$. The parameter space may be reduced by noting that the solution for the temperature in $x < w$ takes the form

$$\theta(x, z; S, \Theta) = 1 - (1 - \Theta) F(x, z; \tilde{S}), \tag{3.14a}$$

where the effective Stefan number $\tilde{S}$ is given by

$$\tilde{S} = (S + \Theta)/(1 - \Theta) \tag{3.14b}$$

and F satisfies (3.13*a*), $F = 0$ at $z = 0$, $F = 1$ at $x = w$ and $F_{x-} = \tilde{S}\dot{c}$.

Equations (3.13) form a simple parabolic system, which is readily integrated from $z = 0$ using a Crank–Nicholson scheme for θ and a Runge–Kutta scheme for w. Some solutions are shown in figure 6. For $z \ll 1$ the solution asymptotes to the similarity solution (3.10). As z increases to $O(1)$ the width of the thermal boundary layer in the fluid increases and occupies the whole channel. The temperature difference between the fluid and the liquidus decreases, as does the rate of melting $-\dot{c}$, and hence the width of the thermal boundary layer in the solid increases rapidly. For $z \gg 1$ the width of the flow tends to a constant value

$$w_\infty = (1 + \tilde{S}^{-1})^{1/3} = \left(\frac{S+1}{S+\Theta}\right)^{1/3} \tag{3.15}$$

and both the temperature excess of the fluid and the rate of melting (figure 6*c*) decay exponentially like $\exp(-pz/w_\infty^4)$, where p is the rate of decay of the lowest eigenmode

Solution	Equations	Requirements
Perturbation	(3.3)	$t^{3/2} \ll z \ll 1$
Error function	(3.4)	$t^{3/2} \ll z \ll t$
Unsteady similarity	(3.8)	$z \ll t$
Steady similarity	(3.10)	$z \ll t^{3/2}, 1$
Steady entry-length	(3.13)	$z \ll t^{3/2}, t^{1/2}$
Liquidus	(3.17)	$1 \ll z \ll t^{1/2}$

TABLE 1. The various asymptotic solutions and their domains of validity for constant-input laminar flows with $\Theta < 1$. Between them the solutions provide a representation of the flow everywhere except when z and t are both $O(1)$.

of the standard, non-solidifying, thermal entry-length problem (Graetz 1885). Thus, as S or Θ decrease and the amount of melting increases, the effective thermal entry length increases like w_∞^4.

It follows from the exponential decay of $\dot{c}$ with z that the width of the boundary layer in the solid for a steady solution increases exponentially with z. However, we know that the temperature in the solid is not steady near the nose of the flow and hence we expect the width of the boundary layer to be no more than $O(t^{1/2})$. Comparison of the estimates of the boundary-layer width suggests that the transient solidification near the nose of the flow ($\Theta > \frac{1}{2}$) gives way to steady melting near the source at $z = z_T$, where

$$z_T = O(w_\infty^4 \ln t/2p). \tag{3.16}$$

It remains to find the solution in $z \gg z_T$. We observe that fluid leaves the region near the source with $\theta = \Theta$ and $w = w_\infty$ to within exponentially small corrections. Hence the solution in the distal region of the flow can be found by a rescaling of the long-time solution obtained in §2.2 for flows initially at the liquidus temperature. Let $\lambda^* = \lambda(S^*)$ denote the solution of (2.2) evaluated at $S^* = S/\Theta$. Then rescaling of (2.18) and use of (3.15) shows that

$$z_N \sim \frac{2}{3\pi} \frac{S+1}{S+\Theta} \frac{t^{1/2}}{\lambda^*}. \tag{3.17}$$

Once again, we find that propagation continues indefinitely, though at an ever-decreasing rate. The asymptotic division of the long-time solution into a nearly steady near-source solution of (3.11) and a near-liquidus far-from-source solution of (2.6) is confirmed by numerical solution of the full system of equations.

We conclude this section with a summary of the asymptotic requirements of the solutions derived (table 1).

4. Time-dependent input with $w(0, t) = t^\alpha$

The foregoing analysis has shown that a flow fed by a constant flux will propagate indefinitely with a length asymptotically proportional to $t^{1/2}$. In contrast, an instantaneous release of a fixed volume will only propagate a finite distance before solidifying completely (Lister 1994). It is natural to ask, therefore, whether flows with a diminishing input flux would propagate for a finite or indefinite distance. Hence, we return to the case $\alpha \neq 0$ in (1.14) and consider flows in which $w(0, t) = t^\alpha$ and the input flux is proportional to $t^{3\alpha}$ (or $t^{(n+1)\alpha}$ in the turbulent case). Since much of the analysis is a simple extension of the methods developed above, we will focus on the results and suppress details of the derivations.

Consider first the case of fluid input at its liquidus temperature ($\Theta = 1$) and allow, for generality, the possibility of non-laminar flow ($n \neq 2$). The requirement that the volume flux be integrable as $t \to 0$ limits the allowable values of α to $\alpha > -1/(n+1)$. It is readily shown that the solution of (2.3) and (2.4) without solidification ($\lambda = 0$) is given by

$$z = w^n(t - w^{1/\alpha}), \tag{4.1a}$$

$$z_N = \frac{\{n(n\alpha+\alpha+1)\}^{n\alpha} t^{n\alpha+1}}{\{(n+1)(n\alpha+1)\}^{n\alpha+1}}. \tag{4.1b}$$

When solidification occurs the equations can be rescaled to remove the solidification rate λ by defining

$$z = Z\lambda^{-2(n\alpha+1)/(1-2\alpha)}, \quad w = W\lambda^{-2\alpha/(1-2\alpha)}, \quad t = T\lambda^{-2/(1-2\alpha)}. \tag{4.2}$$

The width along characteristics is then given by

$$W(T;\phi) = T_S^{\alpha} - \int_{T_S}^{T} \frac{\mathrm{d}v}{[v - T_N[Z(v;\phi)]]^{1/2}} \tag{4.3}$$

from which it is clear that solidification introduces an $O(T^{1/2-\alpha})$ correction to (4.1). Hence solidification can be analysed as a small perturbation if either $\alpha < \frac{1}{2}$ and $T \ll 1$ or $\alpha > \frac{1}{2}$ and $T \gg 1$. We expect solidification to be dominant if the reverse inequalities are satisfied. To confirm this we seek a solution to (2.4) and (2.6*a–c*) analogous to (2.14).

If solidification is dominant then the time for W to decrease from T^{α} to near zero is $O(T^{\alpha+1/2})$. During most of this time W is $O(T^{\alpha})$ and hence $(\partial Z/\partial T)_{\phi}$ is $O(T^{n\alpha})$. Thus the distance propagated along a characteristic during solidification is $O(T^{n\alpha+\alpha+1/2})$. Motivated by these scalings, we set

$$T_N = (kZ)^{1/\gamma}, \quad kZ(T;T_S) = T_S^{\gamma} f(\eta), \tag{4.4a, b}$$

where

$$\eta = k(T - T_S)/T_S^{\alpha+1/2} \quad \text{and} \quad \gamma = (n+1)\alpha + \tfrac{1}{2}. \tag{4.4c, d}$$

Provided $\gamma > 0$ so that T_N is an increasing function of Z then substitution of (4.4) into the characteristic equations and neglect of terms of $O(T^{\alpha-1/2})$ yields

$$kf''/n(f')^{1-1/n} = -1/(1-f^{1/\gamma})^{1/2} \tag{4.5a}$$

$$f(0) = 0, \quad f'(0) = 1, \quad f(\eta_N) = 1, \quad f'(\eta_N) = 0. \tag{4.5b–e}$$

From the first integral

$$\left[\frac{k(f')^{(1/n)+1}}{n+1}\right] = -\int \frac{\mathrm{d}f}{(1-f^{1/\gamma})^{1/2}}$$

and the boundary conditions we find that

$$k = (n+1)\gamma \mathrm{B}(\gamma, \tfrac{1}{2}) \quad (\gamma > 0), \tag{4.6a}$$

where B denotes the beta function

$$\mathrm{B}(a,b) = \int_0^1 v^{a-1}(1-v)^{b-1}\,\mathrm{d}v = \frac{\Gamma(a)\,\Gamma(b)}{\Gamma(a+b)}. \tag{4.6b}$$

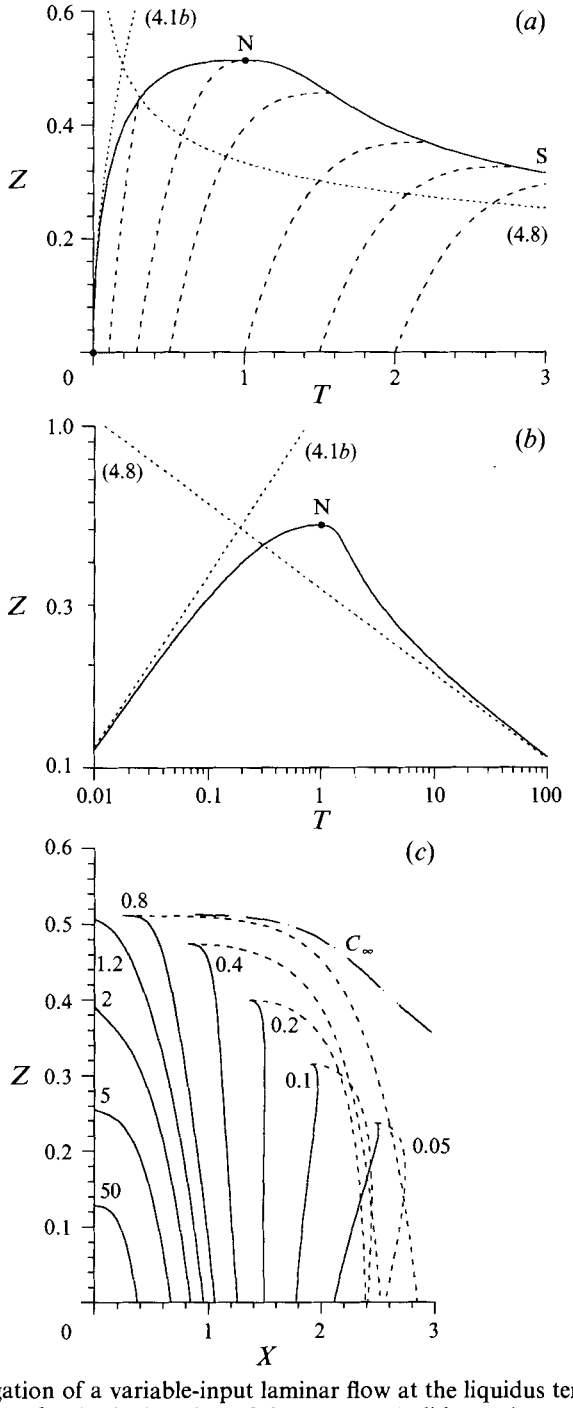

FIGURE 7. The propagation of a variable-input laminar flow at the liquidus temperature ($n = 2$ and $\Theta = 1$) for the case $\alpha = -\frac{1}{4}$. (*a*) The location of the nose Z_N (solid curve) together with some of the characteristics (dashed) used to determine the solution and two asymptotic results (dotted). The nose of the flow freezes completely at N so that $W_N > 0$ along ON and $W = 0$ along NS. (*b*) The source flux decreases sufficiently rapidly that initial advance in which solidification is negligible and $Z_N = 2(\frac{1}{3}T)^{1/2}$ gives way to a long-time retreat of the flow in which solidification is dominant and $Z_N = \frac{1}{3}T^{-1/4}$. The asymptotic solutions (4.1*b*) and (4.8) are shown dotted. (*c*) The scaled width W (solid curves) and accumulated chill thickness C (dashed) as a function of vertical distance Z at various times together with the chill thickness C_∞ left by the receding flow (long dashed). The width decreases monotonically with time due to both the waning source flux and the effects of solidification.

Since the neglected terms are of $O(T^{\alpha-1/2})$, this solution describes the asymptotic behaviour for $T \gg 1$ if $\alpha < \frac{1}{2}$ and for $T \ll 1$ if $\alpha > \frac{1}{2}$.

If $\gamma < 0$ then the expected long-time asymptotic form (4.4*b*) of T_N is a decreasing function of Z. At early times, however, the flow was advancing according to (4.1*b*) and it is this increasing value of T_N that should be used in (2.6*b*). Thus the substitution of (4.4) now yields

$$kf''/n(f')^{1-1/n} = -1 \tag{4.7}$$

since $T_S \gg T_N$, and it is readily shown that

$$f = 1 - \left(1 - \frac{\eta}{n+1}\right)^{n+1}, \quad Z_N = \frac{T^\gamma}{n+1} \quad (\gamma < 0). \tag{4.8}$$

Two critical values of α are apparent from this analysis. First, the propagation of the flow makes a transition from $Z_N \propto T^{n\alpha+1}$ and negligible solidification to $Z_N \propto T^{n\alpha+\alpha+1/2}$ and dominant solidification when $T = O(1)$ (figure 7*a*, *b*), but the direction of the transition depends on whether $\alpha < \frac{1}{2}$ or $\alpha > \frac{1}{2}$. Secondly, in the solidification-dominant regime propagation will only continue indefinitely if $2\alpha > -1/(n+1)$ corresponding to $(\gamma > 0)$. If $2\alpha < -1/(n+1)$ then the nose of the flow solidifies completely at some maximum distance of propagation Z_{max} when $T = O(1)$ and the region of active flow diminishes and is more closely confined to the source (figure 7*c*). Thus this second critical value of α is, in some sense, the marginal case between the indefinite propagation of a constant-flux release and the finite propagation of a constant-volume release.

We turn now to the more general case of fluid input with some superheat ($\Theta < 1$) and restrict attention once more to laminar flow ($n = 2$). As before, the superheat is only significant near the source of the flow, and far from the source the solutions for $\Theta = 1$ can be rescaled to describe the flow. The shear rate in Poiseuille flow is proportional to w and hence the linear shear experienced by the thermal boundary layer at the edges of the flow near the source varies like t^α. A similarity solution analogous to (3.8) can be found, which shows that the transition between solidification and melting now extends away from the source like $t^{\alpha+3/2}$. This solution is appropriate for $T \ll 1$ if $\alpha < \frac{1}{2}$ and for $T \gg 1$ if $\alpha > \frac{1}{2}$. The thermal entry length for Poiseuille flow is proportional to w^4. In the solidification-dominated regime a similarity solution can thus be found for the near-source flow in which the fluid loses its superheat over a length proportional to $t^{4\alpha}$. This solution is appropriate for $T \gg 1$ if $\alpha < \frac{1}{2}$ and for $T \ll 1$ if $\alpha > \frac{1}{2}$.

5. Discussion

There are many natural and industrial processes in which solidification of a hot flow in a cold environment plays an important role. In this paper we have focused on the case of continual input between freely deformable boundaries and found, as discussed below, that both the input and the deformability have significant effects on the behaviour of the flow.

A variety of asymptotic solutions have been obtained, which shed light on the structure of the flow at long and short times, both near and far from the source. The scaled solutions are characterized by the Stefan number S, the dimensionless solidification temperature Θ and the source flux. If the source flux (in laminar flow) is

proportional to $t^{3\alpha}$ then, in the absence of solidification, the distance propagated by the nose of the flow is proportional to $t^{2\alpha+1}$. If $\alpha < \frac{1}{2}$ and $\Theta > \frac{1}{2}$ (or $\Theta < \frac{1}{2}$) then the initial effects of solidification (melting) are small, the thermal contrasts are confined to thin boundary layers and the position of the nose is retarded (advanced) by an amount proportional to $t^{\alpha+3/2}$. If $\Theta < 1$ then the continual supply of superheated fluid prevents the boundary layer in the fluid near the source from thickening with time and causes rapid melting in a near-source region which initially extends in length like $t^{\alpha+3/2}$. However, the superheat of the fluid input is eventually lost to lateral conduction and latent heat over a thermal entry length proportional to $t^{4\alpha}$, which is attained when t and z_N are $O(1)$. At larger times the temperature within the thermal entry length approaches a quasi-steady solution (in scaled coordinates) with melting of the sidewalls, while far beyond the thermal entry length the fluid is at its liquidus temperature and solidifies at a rate proportional to $(t-t_N)^{-1/2}$. The propagation of the nose slows to $t^{3\alpha+1/2}$ and nearly all the fluid supplied solidifies against the sidewalls. This whole sequence of behaviour is simply reversed if the source flux increases with $\alpha > \frac{1}{2}$.

A number of contrasts can be drawn with the evolution of an instantaneous release of fixed volume. Firstly, the near-source structure of the solutions is significantly different. Whereas the narrow width at the base of a constant-volume flow leads to a near-source region of complete solidification proportional to t^2, a continual input leads either to the absence of any special behaviour near the source ($\Theta = 1$) or to a near-source region of melting ($\Theta < 1$). This is an important result for geological applications since melting of the boundaries corresponds to contamination of the original magma by host rock, which may be of quite a different composition. In this context we note that the amount of contamination relative to the original melt approaches $(1-\Theta)/(S+\Theta)$ from (3.15). Secondly, whereas a constant-volume flow ceases to propagate and solidifies completely after a finite time and distance, a flow with constant input will continue to propagate indefinitely, though at an ever decreasing rate. Thirdly, the spatial and temporal pattern of solidification and melting is much simpler for the case of continual input since it consists only of melting near the source and solidification beyond a certain time-dependent distance.

It is perhaps unexpected that a constant-input flow is found to propagate indefinitely. Some insight into this result may be gained by noting that the condition for indefinite propagation is $\alpha > -\frac{1}{6}$ or, equivalently, that the source flux decays no more rapidly than $t^{-1/2}$. If a flow attains a fixed or decreasing length then, since the width of the diffused thermal anomaly in the solid is $O(t^{1/2})$, the total rate of solidification is $O(t^{-1/2})$. Hence, propagation will continue if the source flux is greater than $O(t^{-1/2})$. The sources of magma at the base of the lithosphere are often envisaged as spongy regions of partial melt, while near-surface dykes and lava flows may be fed from inflated chambers of magma. In each case, we expect that the flow rate will decrease as the source region is progressively drained by the flow. This observation coupled with the condition for continued propagation suggests that a decrease in source flux may be the critical factor in determining the duration and extent of geological flows.

It should be noted, however, that some of the assumptions underlying the model equations (1.1)–(1.14) may need to be reassessed at very large times. For constant-input currents the neglect of elastic stresses in the flow walls in comparison to the buoyancy forces remains valid on the scale of the flow since both z_N and c increase like $t^{1/2}$. The chief qualification to the long-time behaviour is thus likely to be that the assumption of large Péclet number must eventually break down locally at the nose of the flow when w_N and $\dot{z}_N$ are sufficiently small. In this regime we must extend the

description of the nose as a frontal shock governed by heat and mass conservation and reintroduce the effects of non-parallel flow and along-stream conduction. Extensive chilling near the forward stagnation point may then be sufficient to stall propagation, though further modelling is required to investigate this possibility.

The results obtained for flow in a conduit with freely deformable walls should be compared with those from previous studies of flows in a rigid-walled conduit (Delaney & Pollard 1982; Bruce & Huppert 1990) in which solidification against the walls reduces the width of the flow and hence the flow rate. Though the methods used to calculate the flow reduction are somewhat approximate in both these studies, there is no reason to question their conclusion that a rigid-walled flow will always choke and solidify if it exceeds a certain multiple of the thermal entry length. The deformability of the boundaries in the present study plays an essential role since it allows the chill to be displaced laterally and flow to continue if sufficient flux is arriving from below.

It would be of general fluid-mechanical interest to extend these calculations to other flow geometries. Generalizations appropriate to lava flows with convective or radiative cooling terms (Fink & Griffiths 1990) were described in Part 1. Alternatively, if the melting temperature of the boundaries were greater than the initial temperature of the fluid then the long-time solution would be a constant-velocity travelling wave of scale given by the thermal entry length and behind which both fluid and solid were close to the input fluid temperature. Finally, it would be of particular geological interest to consider buoyancy-driven flows of finite lateral extent (Lister 1992) and to investigate the channellization of the flow by solidified 'levées' at the lateral margins of the flow where cooling is most rapid.

I am grateful to R. C. Kerr and H. E. Huppert for constructive comments on an earlier version of this manuscript.

Appendix. The temperature in shear flow past a cold wall

Consider a linear shear flow $\boldsymbol{u} = (0, x)$ in $x > 0$ and $z > 0$ past a wall at $x = 0$. For convenience, we reverse our usual temperature scale and let the initial temperature of the fluid be $\theta = 0$ with the wall maintained at temperature $\theta = 1$ and the fluid supply at temperature $\theta = 0$. Solidification, melting and along-stream conduction are not considered. We are thus required to solve

$$\theta_t + x\theta_z = \theta_{xx}, \tag{A 1}$$

$$\theta(x, z, 0) = 0, \quad \theta(x, 0, t) = 0, \tag{A 2a, b}$$

$$\theta(0, z, t) = 1, \quad \theta(\infty, z, t) = 0. \tag{A 2c, d}$$

Equations (A 1) and (A 2) occur as the limit of (3.8) when solidification is negligible ($S \gg 1$) and describe the near-wall ($x' \ll w$), near-source ($z \ll z_N$), short-time ($t \ll 1$) solution of the problem defined by (1.1)–(1.14), which forms the main focus of the body of this paper. However, the problem posed by (A 1) and (A 2) will occur generically in other heat-transfer problems.

As described by Bruce (1989), (A 1) may be solved by taking Laplace transforms with respect to t and z to obtain

$$(s + px)\,\bar{\theta} = \bar{\theta}_{xx}, \tag{A 3}$$

where $\bar{\theta}(x,p,s) = \int\int \theta(x,z,t)\exp(-pz-st)\,\mathrm{d}z\,\mathrm{d}t$. The solution of (A 3) that satisfies the boundary conditions (A 2) is given by

$$\bar{\theta}(x,p,s) = \frac{\mathrm{Ai}\,(sp^{-2/3}+xp^{1/3})}{sp\,\mathrm{Ai}\,(sp^{-2/3})}, \tag{A 4}$$

where Ai denotes the Airy function. The self-similar structure of the solution is revealed by making the substitutions

$$\xi = xt^{-1/2}, \quad \zeta = zt^{-3/2}, \quad \phi = pt^{3/2}, \quad \sigma = st \tag{A 5}$$

to obtain the inversion integral

$$\theta(\xi,\zeta) = \frac{1}{(2\pi\mathrm{i})^2}\int\int \frac{\mathrm{Ai}\,(\sigma\phi^{-2/3}+\xi\phi^{1/3})}{\sigma\phi\,\mathrm{Ai}\,(\sigma\phi^{-2/3})}\exp(\phi\zeta+\sigma)\,\mathrm{d}\sigma\,\mathrm{d}\phi, \tag{A 6}$$

where the contours of integration lie to the right of the poles of the integrand. Integrating with respect to σ, we find that

$$2\pi\mathrm{i}\theta(\xi,\zeta) = \int \phi^{-1}\,\mathrm{Ai}\,(\xi\phi^{1/3})\exp(\phi\zeta)\,\mathrm{d}\phi + \sum_{a_i}\{a_i\,\mathrm{Ai}'(a_i)\}^{-1}\int \phi^{-1}\,\mathrm{Ai}\,(a_i+\xi\phi^{1/3})\exp(\phi\zeta+a_i\phi^{2/3})\,\mathrm{d}\phi, \tag{A 7}$$

where a_i are the zeros of the Airy function and the contours of integration lie to the right of the branch cut on the negative real axis. The first integral in (A 7) can be shown to be equal to the doubly self-similar near-source solution (3.10), but the remainder do not appear to be tractable analytically. Numerical solutions are, of course, available as described in §3.1.

REFERENCES

Bruce, P. M. 1989 Thermal convection within the Earth's crust. PhD Thesis, Cambridge University.

Bruce, P. M. & Huppert, H. E. 1989 Thermal control of basaltic fissure eruptions. *Nature* **342**, 665–667.

Bruce, P. M. & Huppert, H. E. 1990 Solidification and melting in dykes by the laminar flow of basaltic magma. In *Magma Transport and Storage* (ed. M. P. Ryan), Wiley.

Carslaw, H. S. & Jaeger, J. C. 1959 *Conduction of Heat in Solids*. Oxford University Press.

Delaney, P. T. 1987 Heat transfer during emplacement and cooling of mafic dykes. In *Mafic Dyke Swarms* (ed. H. C. Halls & W. H. Fahrig). Geol. Soc. Canada Special Paper 34.

Delaney, P. T. & Pollard, D. D. 1982 Solidification of basaltic magma during flow in a dike. *Am. J. Sci.* **282**, 856–885.

Fink, J. H. & Griffiths, R. W. 1990 Radial spreading of viscous-gravity currents with solidifying crust. *J. Fluid Mech.* **221**, 485–509.

Gradshteyn, I. S. & Ryzhik, I. M. 1980 *Table of Integrals, Series, and Products*. Academic Press.

Graetz, L. 1885 Über die Wärmeleitungsfähigkeit von Flüssigkeiten. *Annalen Physik Chem.* **25**, 337–357.

Hirs, G. G. 1974 A systematic study of turbulent film flow. *J. Lubric. Tech.* **96**, 118–126.

Leveque, M. A. 1928 Les lois de la transmission de chaleur par convection. *Annales Mines Mem.* **13**, 201–299.

Lister, J. R. 1990*a* Buoyancy-driven fluid fracture: similarity solutions for the horizontal and vertical propagation of fluid-filled cracks. *J. Fluid Mech.* **217**, 213–239.

Lister, J. R. 1990*b* Buoyancy-driven fluid fracture: the effects of material toughness and of low viscosity precursors. *J. Fluid Mech.* **210**, 263–280.

Lister, J. R. 1992 Viscous flows down an inclined plane from point and line sources. *J. Fluid Mech.* **242**, 631–653.

LISTER, J. R. 1994 The solidification of buoyancy-driven flow in a flexible-walled channel. Part 1. Constant-volume release. *J. Fluid Mech.* **272**, 21–44.

NEWMANN, J. 1969 Extension of the Leveque solution. *Trans. ASME* C: *J. Heat Transfer* **91**, 177–178.

SPENCE, D. A. & TURCOTTE, D. L. 1990 Buoyancy-driven magma fracture: a mechanism for ascent through the lithosphere and the emplacement of diamonds. *J. Geophys. Res.* **95**, 5133–5139.